Numer. Math. Theor. Meth. Appl.
doi: 10.4208/nmtma.2013.1219nm

Vol. **6**, No. 4, pp. 600-616
November 2013

A Hybrid Immersed Interface Method for Driven Stokes Flow in an Elastic Tube

Yi Li, Sarah A. Williams and Anita T. Layton*

Department of Mathematics, Duke University, Durham, NC 27708-0320, USA.

Received 16 August 2012; Accepted (in revised version) 13 March 2013

Available online 2 October 2013

Abstract. We present a hybrid numerical method for simulating fluid flow through a compliant, closed tube, driven by an internal source and sink. Fluid is assumed to be highly viscous with its motion described by Stokes flow. Model geometry is assumed to be axisymmetric, and the governing equations are implemented in axisymmetric cylindrical coordinates, which capture 3D flow dynamics with only 2D computations. We solve the model equations using a hybrid approach: we decompose the pressure and velocity fields into parts due to the surface forcings and due to the source and sink, with each part handled separately by means of an appropriate method. Because the singularly-supported surface forcings yield an unsmooth solution, that part of the solution is computed using the immersed interface method. Jump conditions are derived for the axisymmetric cylindrical coordinates. The velocity due to the source and sink is calculated along the tubular surface using boundary integrals. Numerical results are presented that indicate second-order accuracy of the method.

AMS subject classifications: 76M20, 65M06, 76D07

Key words: Stokes flow, interface tracking, immersed interface methods, axisymmetric cylindrical coordinates, boundary integrals.

1. Introduction

Many advanced computational techniques have been developed for simulating the motion of an incompressible fluid interacting with flexible immersed structures, often with an eye toward biological applications. Much of the work has been inspired by Peskin's immersed boundary method [17], proposed originally for studying blood flow through a beating heart [16]. The immersed boundary method has since been applied in a wide variety of settings, e.g., [1,3–6,8,9].

The immersed boundary method transfers singular forces from a boundary, or other structure, onto ambient fluid using smooth approximate Dirac delta functions, typically

*Corresponding author. *Email addresses:* yili@math.duke.edu (Y. Li), williams@math.duke.edu (S. A. Williams), alayton@math.duke.edu (A. Layton)

with $\mathcal{O}(h)$ support. Rather than capturing the jump discontinuity in the solution (e.g., pressure) at the immersed boundary, this approach approximates the solution as a continuous function with large gradient. In general, the immersed boundary method computes approximations with first-order spatial accuracy.

An alternative approach that captures the jumps in the solution and its derivatives sharply, and that generates approximations with second-order accuracy, is the immersed interface method developed by LeVeque and Li [11,12]. The immersed interface method is similar to a method developed earlier by Mayo for solving elliptic problems on an irregular domain [14,15]. Both methods are second-order Cartesian grid methods (though higher-order immersed interface methods have been developed [7,13]), with the key idea being the incorporation of known jumps in the solution or its derivatives into the finite difference schemes.

In this work we consider incompressible Stokes flow through a compliant, closed tube, driven by an internal source and sink. The internal source and sink allow us to represent inflow and outflow conditions while using techniques that apply to closed boundaries. Motivated by applications to blood flow through vessels, we take the structure and flow to be axisymmetric.

Our approach is to decompose the pressure and velocity fields into parts due to the tube boundary and due to the source and sink, so that each may be treated with an appropriate method. The tube surface creates a singularly-supported force on the fluid, resulting in an unsmooth solution; we find this part of the solution using the immersed interface method. Meanwhile, the smooth solution due to the source and sink is efficiently calculated along the tube surface via a boundary integral.

This paper is organized as follows: The axisymmetric governing equations for the fluid are detailed in Section 2 below. We describe our hybrid approach, incorporating the immersed interface method and boundary integral method, in Section 3. The jump conditions critical to the immersed interface method are derived for the axisymmetric setting in Section 4, and numerical results are presented in Section 5. Summary and directions for future work are presented in the Section 6.

2. Governing equations

Our aim is to simulate driven Stokes flow in a three-dimensional elastic tube. To take advantage of boundary integral solutions, we model the tube wall, Γ, as a closed surface, e.g., an ellipsoid or closed tube. To represent inflow and outflow conditions in this closed domain, we incorporate an internal source and sink, located at the ends of the tube (see Fig. 1). The impermeable tube is immersed in fluid in the computational domain Ω. In this study, the characteristics of the fluid (i.e., the viscosity) are assumed to be identical inside and outside of the tube.

In the immersed interface method, the fluid velocity and pressure are computed on a fixed, Eulerian grid, while a moving, Lagrangian frame of reference is used to track the location of the interface Γ over time. Our Eulerian grid is described by cylindrical, axisymmetric coordinates. That is, we use coordinates (r,θ,z), but assume that the domain

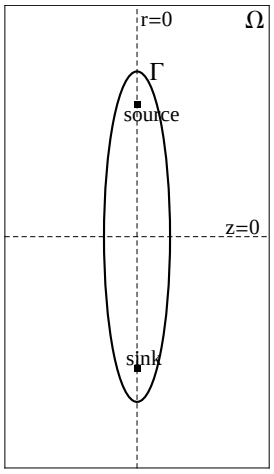

Figure 1: Cross section ($\theta = 0$) of computational domain Ω.

and flow are invariant with θ. In particular, we assume that velocity in the θ direction is always zero. Therefore, the fluid domain reduces to two dimensions, with $\vec{x} = (r,z)$. Furthermore, we compute variable values for the right half of the domain, $r \geq 0$, and enforce symmetry for the left half, $r < 0$. We denote the computed right-half of the domain by $\hat{\Omega}$.

In the axisymmetric cylindrical equations that follow, the vector operator notation refers to the following standard definitions:

$$\nabla p = \Big(\frac{\partial p}{\partial r}, \frac{1}{r}\frac{\partial p}{\partial \theta}, \frac{\partial p}{\partial z}\Big),$$
$$\nabla \cdot (u,v,w) = \Big(\frac{u}{r} + \frac{\partial u}{\partial r}\Big) + \Big(\frac{1}{r}\frac{\partial v}{\partial \theta}\Big) + \frac{\partial w}{\partial z},$$
$$\Delta u = \frac{1}{r}\frac{\partial}{\partial r}\Big(r\frac{\partial u}{\partial r}\Big) + \frac{1}{r^2}\frac{\partial^2 u}{\partial \theta^2} + \frac{\partial^2 u}{\partial z^2}.$$

2.1. Tube surface discretization

The axisymmetric assumption implies that we can represent surface Γ by its cross section at a fixed value of θ, say, $\theta = 0$. We will call the curve found at this cross section Γ as well, with the distinction between curve Γ and surface Γ made clear by context. Curve Γ is represented by markers that move independently of the fixed fluid grid, interpolated by periodic cubic splines. Each marker is labeled by a fixed arclength value s, where s is established as the distance between the marker and an arbitrary origin location under zero source/sink equilibrium conditions. Then $\vec{X} = \big(R(s,t), Z(s,t)\big)$ is the position at time t in (axisymmetric) cylindrical coordinates of the point on Γ whose arclength label is s. We assume that the configuration described by $\vec{X}$ at any time t determines the forces supported

on Γ. The use of splines in the immersed interface method is detailed by Leveque and Li in [12].

2.2. Governing equations

In axisymmetric coordinates, the governing equations for Stokes flow are

$$\mu\Big(\Delta - \frac{1}{r^2}\Big)u - \frac{\partial p}{\partial r} + F_1 = 0, \tag{2.1a}$$

$$\mu\Delta w - \frac{\partial p}{\partial z} + F_3 = 0, \tag{2.1b}$$

$$\nabla \cdot \vec{v} = g. \tag{2.1c}$$

Here velocity $\vec{v} = (u, w)$, p is the pressure, μ is the viscosity (assumed to be constant), and $\vec{F} = (F_1, F_3)$ is given by a surface integral over Γ,

$$F_i = \iint_\Gamma f_i(s,\theta,t)\delta(\vec{x} - \vec{X}(s,\theta,t))dS$$

for $i = 1, 3$, where $\vec{f} = (f_1, f_3)$ denotes the body force (singularly supported) in the r and z directions induced by Γ. Free space boundary conditions are assumed.

Applying the divergence operator to Eqs. (2.1a) and (2.1b), and substituting from Eq. (2.1c), we can also write

$$\Delta(p - \mu g) = \nabla \cdot \vec{F}. \tag{2.2}$$

2.3. Definition of source and sink terms

Rather than enforcing incompressibility everywhere, Eq. (2.1c) describes the source and sink that drive flow through the tube. For compact regions $\vec{x}_{source}$ and $\vec{x}_{sink}$, we have

$$\begin{aligned} g(\vec{x},t) &\geq 0, && \text{for } \vec{x} \in \vec{x}_{source}, \\ g(\vec{x},t) &\leq 0, && \text{for } \vec{x} \in \vec{x}_{sink}, \\ g(\vec{x},t) &= 0, && \text{otherwise.} \end{aligned}$$

We let $\vec{x}_{source}$ be the cylindrical region centered at a point (r_0, z_0) (with $r_0 = 0$ for symmetry about the z axis) such that $|r - r_0| \leq \kappa$ and $|z - z_0| \leq \kappa$ (and $0 \leq \theta < 2\pi$), for fixed radius parameter κ. The region $\vec{x}_{sink}$ is similarly defined.

For $(r,z) \in \vec{x}_{source}$ we define

$$g(t,r,z) = A(t)h_1(r)h_2(z) \tag{2.3}$$

with the following properties:

$$\int_0^{2\pi}\int_0^{\kappa} h_1(r)\cdot r\,dr\,d\theta = 1, \tag{2.4a}$$

$$\int_{-\kappa}^{\kappa} h_2(z)dz = 1. \tag{2.4b}$$

We use cosine functions scaled to meet these criteria:

$$h_1(r) = \beta(\kappa)\Big(1+\cos\Big(\frac{\pi(r-r_0)}{\kappa}\Big)\Big), \tag{2.5a}$$

$$h_2(z) = \frac{1}{2\kappa}\Big(1+\cos\Big(\frac{\pi(z-z_0)}{\kappa}\Big)\Big), \tag{2.5b}$$

where constant $\beta(\kappa)$ is chosen such that Eq. (2.4a) is satisfied. As an example of the magnitude function $A(t)$, in Section 5.2 we use

$$A(t) = 0.0025(1.0+\sin(\omega t - 0.5\pi))$$

for various frequency values ω. We define $g(\vec{x}_{sink}, t)$ similarly but with opposite magnitude, so there is no net accumulation of fluid in the tube, and for other values of $\vec{x}$ we have $g(\vec{x}, t) = 0$.

2.4. Domain boundary conditions

Free space boundary conditions are assumed for the Stokes flow. To discretize the model equations, we impose the following conditions on the half-plane computational domain $\hat{\Omega}$.

Across the z axis, homogeneous Neumann boundary conditions are implemented for pressure and for velocity in the z direction,

$$\frac{\partial p}{\partial r} = 0 \quad \text{and} \quad \frac{\partial w}{\partial r} = 0 \quad \text{at } r = 0, \tag{2.6}$$

and for velocity in the r direction we have

$$u = 0 \quad \text{at } r = 0. \tag{2.7}$$

The other three sides of the domain have Dirichlet boundary conditions for p, u, and w, with values obtained from boundary integrals (Eqs. (3.5), (3.6)) below.

3. Problem decomposition and solution methods

We decompose the pressure and velocity into parts induced by the tube boundary and induced by the source and sink,

$$p = p_{bd} + p_s, \tag{3.1a}$$

$$\vec{v} = \vec{v}_{bd} + \vec{v}_s, \tag{3.1b}$$

so that each may be treated with an appropriate method. The tube boundary creates a singularly-supported force; this part of the solution is addressed by the immersed interface method. The smooth solution due to the source and sink is calculated with a boundary integral method.

3.1. Solution induced by the tube boundary

The pressure and velocity due to the immersed tube boundary, p_{bd} and $\vec{v}_{bd}$, satisfy the equations of Stokes flow, Eqs. (2.1a), (2.1b), and (2.1c), in the absence of source and sink terms, i.e., with $g(\vec{x},t)\equiv 0$. That is,

$$\mu\Big(\Delta-\frac{1}{r^2}\Big)u_{bd}-\frac{\partial p_{bd}}{\partial r}+F_1=0, \tag{3.2a}$$

$$\mu\Delta w_{bd}-\frac{\partial p_{bd}}{\partial z}+F_3=0, \tag{3.2b}$$

$$\nabla\cdot\vec{v}_{bd}=0. \tag{3.2c}$$

Forcing terms that are singularly supported on the tube boundary make this system suitable for the immersed interface method.

3.1.1. Immersed interface method

For the immersed interface method the Stokes equations are recast as a sequence of three Poisson problems. Each is solved by a standard finite difference method, with the discretized right-hand side of each problem determined by jump conditions.

Taking the divergence of Eqs. (3.2a), (3.2b) and applying Eq. (3.2c), p_{bd} satisfies

$$\Delta p_{bd}=\nabla\cdot\vec{F}, \tag{3.3}$$

which is discretized using a standard five-point stencil,

$$\frac{1}{h^2}\left(p_{bd\,i+1,j}+p_{bd\,i-1,j}+p_{bd\,i,j+1}+p_{bd\,i,j-1}-4p_{bd\,i,j}\right)=b_{i,j}. \tag{3.4}$$

Away from the immersed boundary, right-hand side $b_{i,j}=0$, and when the stencil includes points from both sides of the boundary, the immersed interface method prescribes values of $b_{i,j}$ based on jump conditions, as detailed in [11] and [12]. We derive jump conditions for the axisymmetric setting in Section 4; see Eqs. (4.8a) and (4.8b) below.

With values of p_{bd} given, Eqs. (3.2a) and (3.2b) are also Poisson problems with singularly supported right-hand side (F_1 and F_3, respectively), subject to the same finite difference approach incorporating jump conditions. The jump conditions for velocity are given in Eqs. (4.14) and (4.15).

3.1.2. Boundary conditions

Boundary conditions are needed to solve the Poisson problems given above.

Eq. (3.3) has a boundary integral solution, given by

$$p_{bd}=\iint_{\Gamma}-\frac{1}{4\pi}\vec{f}\cdot\nabla\Big(\frac{1}{r}\Big)dS, \tag{3.5}$$

where Γ denotes the (two-dimensional) immersed surface and dS is the surface element.

We make use of the boundary integrals in 3-D Cartesian coordinates to compute solutions for Eqs. (3.2a) and (3.2b). Relating the r component of velocity in cylindrical coordinates to the x and y components of velocity in 3-D Cartesian coordinates, we have

$$u^{\text{cylindrical}} = u^{\text{Cartesian}} \cos(\theta) + v^{\text{Cartesian}} \sin(\theta).$$

When $\theta = 0$, the statement reduces to

$$u^{\text{cylindrical}} = u^{\text{Cartesian}}.$$

Therefore, we can make use of the boundary integral solution for Cartesian coordinates to obtain the boundary value of u, as well as w (which is unchanged in Cartesian coordinates). Using the notation $\vec{x}' = (x_1', x_2', x_3')$, we have

$$\vec{v}_{bd}^{\text{Cartesian}} = \iint_{\Gamma} \frac{1}{8\pi\mu} \Big(\frac{\delta_{ij}}{r} + \frac{x_i' x_j'}{r^3} \Big) f_j dS(x'). \tag{3.6}$$

3.2. Solution induced by the source and sink

The part of the pressure solution due to the source and sink is determined by comparing Eqs. (3.3) and (2.2):

$$p_{bd} = p - \mu g, \tag{3.7}$$

so

$$p_s = \mu g.$$

For velocity, our decomposition produces

$$\Big(\Delta - \frac{1}{r^2} \Big) u_s = \frac{1}{\mu} \frac{\partial p_s}{\partial r} = \frac{\partial g}{\partial r}, \tag{3.8a}$$

$$\Delta w_s = \frac{1}{\mu} \frac{\partial p_s}{\partial z} = \frac{\partial g}{\partial z}. \tag{3.8b}$$

These equations have smooth solutions which would typically be computed with a finite difference approach. However, the $1/r^2$ term in Eq. (3.8a) grows large as $r \to 0$. Furthermore, when g's radius parameter κ is on the order of grid spacing h, $\partial p_s / \partial r$ is also large near $r = 0$. This is because the maximum of g is found at $r = 0$ and $g(t, r, z) \approx 0$ for $r = \kappa$. These two large terms generate large numerical errors in a finite difference scheme; instead we use a boundary integral method to evaluate $\vec{v}_s$ on the immersed interface. We don't have the boundary integral solution for u_s directly from Eq. (3.8a), but we can refer to the solution for Cartesian coordinates as we did for Eq. (3.2a) above.

The relevant equation in 3-D Cartesian coordinates is

$$\Delta \vec{v}_s = \nabla g, \tag{3.9}$$

which has boundary integral solution

$$\vec{v}_s^{\text{Cartesian}} = \iiint_{\Omega} \frac{1}{4\pi} \frac{\nabla g(x')}{r} dV(x'), \tag{3.10}$$

where Ω is the (three-dimensional) computational domain and dV denotes the volume element. To evaluate Eq. (3.10) we need the source/sink function g in Cartesian coordinates; in Eq. (2.3), g is given in axisymmetric coordinates. We simply use a Cartesian grid with x axis and z axis identical to the r and z axes of our axisymmetric cylindrical fluid grid.

3.3. Overview of hybrid computational approach

We briefly summarize the approach detailed in the previous sections. At time t^n, approximate values are known for marker locations $\vec{X}(s,t^n)$, establishing the configuration of tube surface Γ. To advance the system to time t^{n+1}:

1. *Dirichlet boundary conditions:* Compute p_{bd}, u_{bd} and w_{bd} (values due to tube boundary force) on the boundary of domain Ω using boundary integrals (3.5) and the first and third components of (3.6).
2. *Advance $\vec{v}_{bd}$ and p_{bd} via immersed interface method:*
   (a) Using a cubic spline representation of the boundary force $\vec{f}$ along Γ, calculate jump condition corrections from Eqs. (4.8a) and (4.8b) for pressure, and Eqs. (4.14) and (4.15) for velocity.
   (b) Incorporate jump conditions into finite difference approximations for p_{bd}^{n+1} and $\vec{v}_{bd}^{n+1}$ on the fluid grid.
3. *Find velocity due to source and sink via boundary integral:* Use Eq. (3.10) to find $\vec{v}_s^{n+1}$ (velocity field due to source and sink) on the tube boundary markers.
4. *Advance location of tube surface Γ:*
   (a) Advance tube boundary markers, i.e., find $\vec{X}(s,t^{n+1})$, according to the total velocity field, $\vec{v} = \vec{v}_{bd} + \vec{v}_s$:

$$\vec{X}(s,t^{n+1}) = \vec{X}(s,t^n) + \Delta t\Big(\frac{3}{2}\vec{v}\big(\vec{X}(s,t^n),t^n\big) - \frac{1}{2}\vec{v}\big(\vec{X}(s,t^{n-1}),t^{n-1}\big)\Big). \tag{3.11}$$

   Boundary velocity is extrapolated from previous time-levels because while v^{n+1} is known at grid points, X^{n+1} has yet to be computed.

   (b) Update $\vec{v}_{bd}^{n+1}$ on boundary marker locations, using a second order interpolation scheme that incorporates the jump in velocity across the immersed boundary (see [12]).

4. Derivation of jump conditions for axisymmetric coordinate system

Next we derive the jump conditions for pressure and velocity for Stokes flow in the axisymmetric cylindrical coordinate system. Note that the divergence-free flow described in this section corresponds to the part of the solution due to the immersed boundary discussed in Section 3.1. For ease of notation, however, rather than using the variables p_{bd} and $\vec{v}_{bd}$ in this section, we use generic p, u, v, w without the subscript bd.

We consider momentarily the governing equations in fully three-dimensional cylindrical coordinates, then apply the assumption of invariance with θ to derive jump conditions for the axisymmetric setting.

The equations governing Stokes flow in 3-D cylindrical coordinates are

$$\mu\Big(\Delta - \frac{1}{r^2}\Big)u - \frac{2\mu}{r^2}\frac{\partial v}{\partial \theta} - \frac{\partial p}{\partial r} + F_1 = 0, \tag{4.1a}$$

$$\mu\Big(\Delta - \frac{1}{r^2}\Big)v + \frac{2\mu}{r^2}\frac{\partial u}{\partial \theta} - \frac{1}{r}\frac{\partial p}{\partial \theta} + F_2 = 0, \tag{4.1b}$$

$$\mu\Delta w - \frac{\partial p}{\partial z} + F_3 = 0, \tag{4.1c}$$

$$\nabla \cdot \vec{v} = 0, \tag{4.1d}$$

where $\vec{x} = (r, \theta, z)$, $\vec{v} = (u, v, w)$, and $\vec{F} = (F_1, F_2, F_3)$, with

$$F_i = \iint_\Gamma f_i(s, \theta, t)\delta(\vec{x} - \vec{X}(s, \theta, t))dS \tag{4.2}$$

for $i = 1, 2, 3$. Taking the divergence of Eqs. (4.1a), (4.1b), (4.1c) yields a Poisson equation for pressure,

$$\Delta p = \nabla \cdot \vec{F}. \tag{4.3}$$

Let $\psi(r, \theta, z)$ be an arbitrary twice continuously differentiable test function. Multiplying ψ on the right hand side of Eq. (4.3), and applying Green's theorem, we have

$$\begin{aligned}\iiint_\Omega (\nabla \cdot \vec{F})\psi(r, \theta, z)dV &= \iiint_\Omega \Big(\iint_\Gamma (\nabla \cdot \vec{f}(s, \theta, t)\delta(\vec{x} - \vec{X}(s, \theta, t))dS\Big)\psi(r, \theta, z)dV \\ &= -\iint_\Gamma \Big(f_1\frac{\partial \psi}{\partial r} + \frac{f_2}{r}\frac{\partial \psi}{\partial \theta} + f_3\frac{\partial \psi}{\partial z}\Big)dS.\end{aligned} \tag{4.4}$$

By using (s, θ) coordinates to parameterize surface Γ, the surface element is $dS = rdsd\theta$.

Let Γ^+ be a region that encloses the boundary surface Γ, and let the distance between Γ^+ and Γ shrink to zero. As $\Gamma^+ \to \Gamma$, multiplying $\psi(r, \theta, z)$ on the left hand side of Eq. (4.3) and applying Green's theorem again, we have

$$\iiint_{\Gamma^+} (\Delta p)\psi dV \to 2\pi\Big(\int_\Gamma \Big[\frac{\partial p}{\partial n}\Big]\psi r ds - \int_\Gamma [p]\psi_n r ds\Big). \tag{4.5}$$

Here n is the outward normal direction and ds is the arclength element.

Now we make explicit our axisymmetric assumptions, that ψ and f are independent of θ. Then Eq. (4.4) can finally be written as

$$\iiint_{\Omega} (\nabla \cdot \vec{F})\psi(x,y)dV = -2\pi \int_{\Gamma} \Big(f_1 \frac{\partial \psi}{\partial r} + f_3 \frac{\partial \psi}{\partial z}\Big) r ds. \tag{4.6}$$

Here Γ denotes the boundary of the cross section of the surface for fixed θ.

Now we split the force due to the boundary into components tangent to and normal to the boundary. Because

$$f_1 \frac{\partial \psi}{\partial r} + f_3 \frac{\partial \psi}{\partial z} = f_n \frac{\partial \psi}{\partial r} + f_s \frac{\partial \psi}{\partial s},$$

the right hand side of Eq. (4.6) can be written as

$$\int_{\Gamma} \Big(f_1 \frac{\partial \psi}{\partial r} + f_3 \frac{\partial \psi}{\partial z}\Big) r ds = \int_{\Gamma} \Big(f_n \frac{\partial \psi}{\partial n} + f_s \frac{\partial \psi}{\partial s}\Big) r ds = \int_{\Gamma} \Big(f_n r \frac{\partial \psi}{\partial n} - \frac{\partial (f_s r)}{\partial s}\psi\Big) ds. \tag{4.7}$$

The second step of Eq. (4.7) is obtained by integration by parts on s. Finally, using the fact ψ is arbitrary and combining Eq. (4.6) and Eq. (4.7), the jump conditions for pressure are

$$[p] = f_n, \tag{4.8a}$$

$$\Big[\frac{\partial p}{\partial n}\Big] = \frac{1}{r}\frac{\partial (f_s r)}{\partial s}. \tag{4.8b}$$

To obtain the jump condition for velocity, we can multiply test function ψ on Eq. (4.1a), and integrate:

$$\iiint_{\Gamma^+} \mu(\Delta u)\psi dV - \iiint_{\Gamma^+} \mu\Big(\frac{u}{r^2}\Big)\psi dV - \iiint_{\Gamma^+} \frac{\partial p}{\partial r}\psi dV = -\iint_{\Gamma} f_1 \psi dS. \tag{4.9}$$

Next we examine each term on the left-hand side of Eq. (4.9) as $\Gamma^+ \to \Gamma$. For the first term of Eq. (4.9) we have

$$\iiint_{\Gamma^+} \mu(\Delta u)\psi dV \to \iint_{\Gamma} \Big[\mu \frac{\partial u}{\partial n}\Big]\psi dS. \tag{4.10}$$

The second term of Eq. (4.9) is

$$\iiint_{\Gamma^+} \mu\Big(\frac{u}{r^2}\Big)\psi dV = \iiint_{\Gamma^+} \mu\Big(\frac{u}{r^2}\Big)\psi r dr d\theta dz = \iiint_{\Gamma^+} \mu\Big(\frac{u}{r}\Big)\psi dr d\theta dz. \tag{4.11}$$

Now we enforce our axisymmetric assumptions and conclude that the second term vanishes as $\Gamma^+ \to \Gamma$: if $r \to 0$, then $u \to 0$ in the axisymmetric cylindrical coordinate system. On the other hand, when r remains finite, $|u/r| \to |\partial u/\partial r|$, which remains bounded Therefore, as $\Gamma^+ \to \Gamma$, the second term of Eq. (4.9) vanishes, whether $r \to 0$ or not.

The third term of Eq. (4.9) is

$$\iiint_{\Gamma^+} \frac{\partial p}{\partial r}\psi dV = \iint_{\Gamma^+} \psi\Big(\nabla\cdot[p,0] - \frac{p}{r}\Big)dV. \tag{4.12}$$

As $\Gamma^+ \to \Gamma$,

$$\iiint_{\Gamma^+} \psi\nabla\cdot[p,0]dS \to \iint_{\Gamma} \psi[p]\cos(\alpha)dS, \tag{4.13a}$$

$$\iiint_{\Gamma^+} \psi\frac{p}{r}dS \to 0. \tag{4.13b}$$

Here α is the angle between the normal and r direction. Therefore, we have the jump for u,

$$\Big[\mu\frac{\partial u}{\partial n}\Big] = [p]\cos\alpha - \frac{f_1}{|f_1|} = f_s\sin\alpha. \tag{4.14}$$

Similarly, we can derive the jump for w, which is

$$\Big[\mu\frac{\partial w}{\partial n}\Big] = [p]\sin\alpha - \frac{f_3}{|f_3|} = -f_s\cos\alpha. \tag{4.15}$$

5. Numerical results

Our method has second order spatial accuracy in the absence of source and sink, shown below in Section 5.1, and the simulated flow is found to be approximately Poiseulle (Section 5.2.1). We also study the behavior of the fluid field under oscillating inflow and outflow. Although complicated fluid behavior has previously been observed for pumped Navier-Stokes flow, (e.g., [8]), in our Stokes flow study the amplitude of pressure and velocity fluctuations decrease as the forcing oscillations increase in frequency (Section 5.2.2). We also investigate inflow/outflow oscillations of increasing frequency under controlled, steady pressure.

5.1. Convergence test

To demonstrate the second order spatial accuracy of our method, we consider a spherical elastic surface deformed into an ellipsoid shape. (This stationary example does not include a source and sink.) At the plane $\theta = 0$, the cross section of the ellipsoid is described parametrically as $(0.8\cos(\phi), 0.6\sin(\phi))$. The equilibrium shape for this surface cross section is a circle with radius 0.7, centered at origin. In this example, the fluid domain is $[-1.8, 1.8]\times[-1.8, 1.8]$, and the fluid field is computed for $N = 40, 80, 160$, and 320, with uniform grid spacing $h = 3.6/N$ in each case. The immersed boundary is discretized using 240 markers. We use the solution computed on a high-resolution 640×640 grid as the reference solution to estimate errors. Table 1 displays the convergence results, where the velocity columns average the results in the r and z directions.

Table 1: Convergence results for p and $\vec{v}$. Approximations exhibit second-order convergence.

	p		$\vec{v}$	
N	L_1 error/h^2	L_{inf} error/h^2	L_1 error/h^2	L_{inf} error/h^2
40	1.012e-2	8.932e-1	1.600e-2	1.362e-1
80	1.098e-2	6.470e-1	1.420e-2	1.058e-1
160	8.221e-3	9.818e-1	1.109e-2	1.045e-1
320	4.849e-3	1.405	9.415e-3	1.036e-1

5.2. Oscillating inflow

Here we simulate the motion of a compliant tube with an internal source and sink that introduce an oscillating pumping force. In this example, the tube wall is subject to elastic tension and tether forces.

The fluid domain is $[-0.45, 0.45] \times [-3.6, 3.6]$, with the $r \geq 0$ half of the domain discretized on a 40×640 grid (and the $r < 0$ half reflected), so grid spacing $h = 0.01125$. The time step for the simulation is $h/20$.

Fig. 2 shows the configuration of the tube. The source and sink are centered at $(r,z) = (0.0, 2.0)$ and $(r,z) = (0.0, -2.0)$, respectively, with radius parameter $\kappa = h = 0.0225$. At equilibrium, the top of the tube is the upper half of the circle with radius 0.2 centered at the source, described by

$$r^2 + (z - 2.0)^2 = 0.2^2.$$

Similarly, the bottom of the tube is the lower half of the circle with radius 0.2 centered at the sink:

$$r^2 + (z + 2.0)^2 = 0.2^2.$$

Each half circle is discretized by 8 markers. The left and right walls of the tube are straight lines at equilibrium, $r = 0.2$ and $r = -0.2$ between $z = -2.0$ and $z = 2.0$, with 36 markers on each side. Of the 88 markers, the positions of the 44 on the right half of the domain are computed, while the corresponding markers on the left half of the domain move according to symmetry. We use the notation $\vec{X}(s,t)$ to denote the position (r,z) of the marker associated with equilibrium arclength value s, at time t, and we use $\vec{X}(s_{opp}, t)$ to denote the position of the mirrored twin marker.

The boundary force along the tube surface is composed of two parts,

$$\vec{f} = \vec{f}_e + \vec{f}_t.$$

The elastic tension force is given by

$$\vec{f}_e = \frac{\partial T}{\partial \vec{\tau}} \vec{\tau} - 2T\kappa\vec{n},$$

where $\vec{\tau}(s,t)$ is the tangent vector to the tube surface, $T(s,t)$ is the tension

$$T(s,t) = T_0\Big(\Big|\frac{\partial \vec{X}}{\partial s_0}\Big| - 1\Big),$$

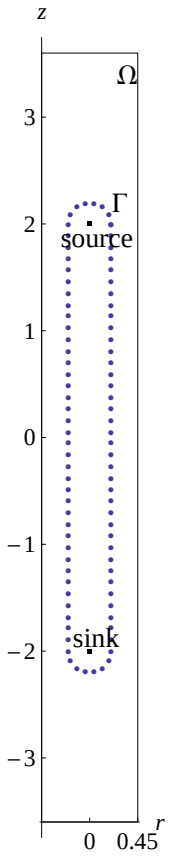

Figure 2: Markers delineate the boundary of an elastic tube.

where s_0 denotes the material coordinate (we use elasticity constant $T_0 = 0.2$). κ denotes the mean curvature, taken positive for a sphere. A derivation for the tension force in cylindrical coordinates can be found in [10].

The tether force $\vec{f}_t$ is defined in two ways. Along the top and bottom semi-circular regions of Γ,

$$\vec{f}_t = -k(\vec{X} - \vec{X}_{eq}),$$

with spring force $k = 100$ and $\vec{X}_{eq}$ the equilibrium position described above.

Along the side regions of the tube, the r and z components of the tether force are defined independently:

$$\vec{f}_t = \begin{bmatrix} f_{rt} \\ f_{zt} \end{bmatrix}, \tag{5.1}$$

where f_{zt} is the z component of the tether force defined above, and f_{rt} arises from a boundary point's elastic connection to its neighbors along the circumference of the tube.

This width-restoring force is defined as

$$f_{rt} = m\big(\big|\vec{X}(s,t) - \vec{X}(s_{opp},t)\big| - L_T\big). \tag{5.2}$$

Here L_T is the equilibrium width of the tube, and m is the force constant. In this example, $L_T = 0.4$ and $m = 50$.

The fluctuating magnitude for the source is

$$A(t) = 0.0025\big(1.0 + \sin(\omega t - 0.5\pi)\big). \tag{5.3}$$

The magnitude for the sink is $-A(t)$. We examine the flow subject to varying fluctuation frequencies ω in Section 5.2.2 below.

5.2.1. Velocity and shear stress

In this example, we choose inflow/outflow oscillation frequency $\omega = 5$. After the system reaches equilibrium, we plot the z direction velocity and shear stress along the cross section $z = 0.99$ (results are qualitatively similar at other cross sections). From the parabolic shape of the z-velocity (Fig. 3(a)), and the v-shaped shear stress (Fig. 3(b)), we can see that the flow is approximately Poiseuille flow, as could be expected for laminar flow through a roughly circular pipe.

To illustrate aspects of the fluid dynamics, we plot in Fig. 4 snapshots of the z-component of the fluid velocity, computed at $z = 0.99$, at five time points. These time points were chosen to be approximately π/ω apart with a period of the inflow/outflow oscillations. The magnitude of the r-component of the fluid velocity is at least an order of magnitude smaller.

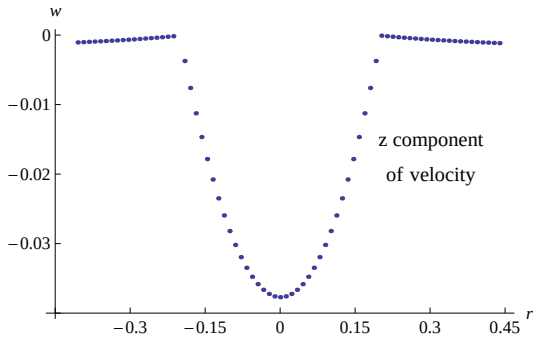

(a) Velocity in the z direction at $z = 0.99$. Approximately parabolic profile is characteristic of Poiseuille flow.

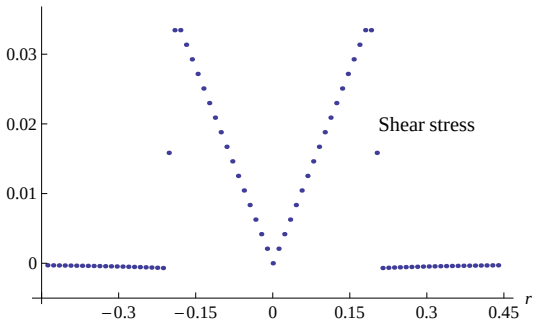

(b) Shear stress at $z = 0.99$. V-shape is characteristic of Poiseuille flow.

Figure 3: Characteristics of Poiseuille flow.

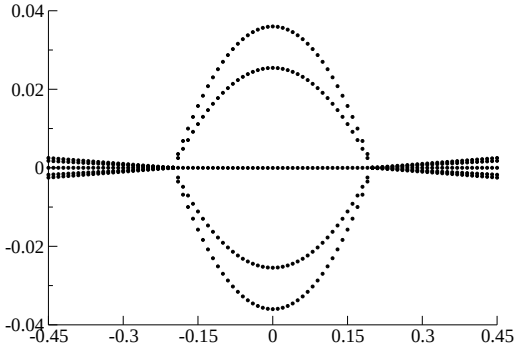

Figure 4: Snapshots of z-component of velocity at $z = 0.99$, sampled at five time-points with a forcing period, ordered in time from bottom to top.

5.2.2. Frequencies and amplitude

Other studies (e.g., [8]) have demonstrated pumped flow that changes nonlinearly with forcing function frequency, even reversing direction for certain frequency ranges. In the current, simple case of Stokes flow, however, we see pressure and flow fields that settle (fluctuation amplitudes decrease) as the pumping speed increases. The data in this set of experiments was collected at $z = 1.8$ and $z = 0.99$, but results are qualitatively similar at other locations.

Fig. 5(a) shows the maximum and minimum pressure values recorded over an equilibrium temporal cycle at point $(r,z) = (0,1.8)$, for increasing pumping frequency. For pumping frequencies $5 \leq \omega \leq 80$, the amplitude of the pressure cycle decreases monotonically.

Fig. 5(b) shows the maximum and minimum flow values obtained by integrating the vertical velocity field at $z = 0.99$ throughout an equilibrium temporal cycle. For all pumping frequencies, fluid flows in the downward direction. For pumping frequencies

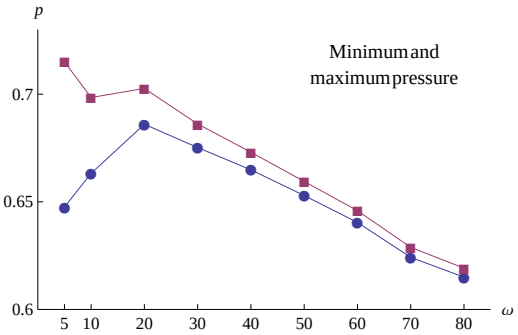

(a) Minimum and maximum of pressure cycle at $(r,z) = (0,1.8)$; pumping frequency $5 \leq \omega \leq 80$.

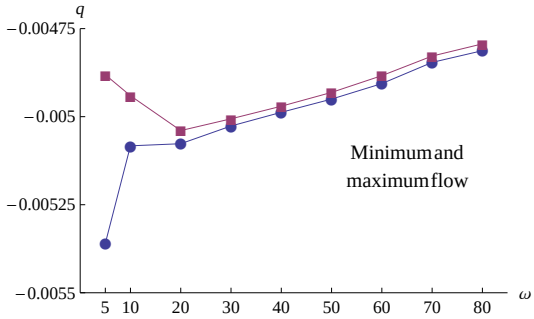

(b) Minimum and maximum of flow across $z = 0.99$ for pumping frequency $5 \leq \omega \leq 80$.

Figure 5: Flow settles as pumping speed increases.

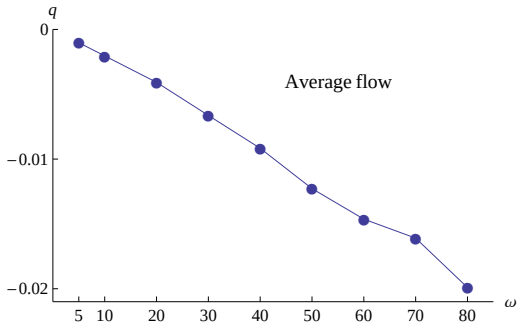

Figure 6: Under increasing pumping frequency and approximately steady pressure, the average flow at $z = 0.99$ increases in absolute value.

$5 \leq \omega \leq 40$, the amplitude of the flow cycle decreases monotonically. For higher pumping frequencies, the amplitude of the flow cycle stays within 0.25% of the mean flow.

Finally, for a more biologically or physically relevant experiment to investigate the effect of pressure fluctuation frequency on flow rate, we varied the frequency of pumping (and therefore the frequency of pressure oscillations) while holding the pressure amplitude approximately fixed ($\approx 1.378 \times 10^{-2}$). To obtain steady pressure amplitude near the source, we adjust the magnitude of inflow/outflow function $A(t)$ (see Eq. (5.3)) as we vary ω. Fig. 6 shows that, under increasing pumping frequency and approximately steady pressure, the average flow at $z = 0.99$ increases in absolute value.

6. Discussion

We have developed a numerical method for simulating Stokes flows along a compliant, closed tube. Fluid motion is described in cylindrical coordinates and is assumed to be axisymmetric. Our approach is based on the immersed interface method and boundary integrals, and robustly captures the jumps in the solution and its derivatives. Jump conditions were derived for the axisymmetric cylindrical coordinates. We used the method to simulate fluid flow through an elastic tube driven by oscillatory forcings, and we studied how the pressure and velocity oscillation amplitudes vary as functions of the forcing frequency.

The present method was developed for Stokes flow and is applicable to creeping flows or fluid with sufficiently high viscosity. However, blood flow in arteries and arterioles has medium to high Reynolds numbers, and thus is more appropriately described as Navier-Stokes flow. To extend the present method to the Navier-Stokes equations, one may use the velocity decomposition approach developed by Layton and Beale [2]. That method, developed for Cartesian coordinates, decomposes the overall solution to the Navier-Stokes equations into a singular piece that satisfies the Stokes equations with singular forces, and a remainder piece that is sufficiently regular to be solved using standard finite difference methods. The singular piece can be computed using the method introduced in the present study.

Acknowledgments This work was supported in part by the National Science Foundation under Grant DMS-0715021.

References

[1] K. M. Arthurs, L. C. Moore, C. S. Peskin, E. B. Pitman, and H. E. Layton, *Modeling arteriolar flow and mass transport using the immersed boundary method*, J. Comput. Phys., 147 (1998), pp. 402–440.

[2] J. T. Beale and A. T. Layton, *A velocity decomposition approach for moving interfaces in viscous fluids*, J. Comput. Phys., 2009.

[3] R. P. Beyer, *A computational model of the cochlea using the immersed boundary method*, J. Comput. Phys., 98 (1992), pp. 145–162.

[4] R. Dillon, L. Fauci, and D. Gaver III, *A microscale model of bacterial swimming, chemotaxis, and substrate transport*, J. Theor. Biol., 177 (1995), pp. 325–340.

[5] L. Fauci and A. McDonald, *Sperm mobility in the presence of boundaries*, Bull. Math. Biol., 57 (1995), pp. 679–699.

[6] A. L. Fogelson, *A mathematical model and numerical method for studying platelet adhesion and aggregation during blood clotting*, J. Comput. Phys., 56 (1984), pp. 111–134.

[7] K. Ito, Y. Kyei, and Z. Li, *Higher-order Cartesian grid based finite difference schemes for elliptic equations on irregular domains*, SIAM J. Sci. Comput., 27(1) (2005), pp. 346–367.

[8] E. Jung, S. Lim, W. Lee, and S. Lee, *Computational models of valveless pumping using the immersed boundary method*, Comput. Methods Appl. Mech. Eng., 197 (2008), pp. 2329–2339.

[9] Y. Kim, M-C Lai, and CS Peskin, *Numerical simulations of two-dimensional foam by the immersedboundary method*, J. Comput. Phys., 229 (2010), pp. 5194–5207.

[10] MC Lai, CY Huang, and YM Huang, *Simulating the axisymmetric interfacial flows with insoluble surfactant by immsered boundary method*, Int. J. Numer. Anal. Model, 8 (2011), pp. 105–117.

[11] R. J. LeVeque and Z. Li, *The immersed interface method for elliptic equations with discontinuous coefficients and singular sources*, SIAM J. Numer. Anal., 31 (1994), pp. 1019–1044.

[12] R. J. LeVeque and Z. Li, *Immersed interface methods for Stokes flow with elastic boundaries or surface tension*, SIAM J. Sci. Comput., 18(3) (1997), pp. 709–735.

[13] M. N. Linnick and H. F. Fasel, *A high-order immersed interface method for simulating unsteady incompressible flows on irregular domains*, J. Comput. Phys., 204 (2005), pp. 157–192.

[14] A. Mayo, *The fast solution of Poisson's and the biharmonic equations on irregular regions*, SIAM J. Numer. Anal., 21 (1984), pp. 285–299.

[15] A. Mayo and A. Greenbaum, *Fast parallel iterative solution of Poisson's and the biharmonic equations on irregular regions*, SIAM J. Sci. Comput., 13 (1982), pp. 101–118.

[16] C. S. Peskin, *Numerical analysis of blood flow in the heart*, J. Comput. Phys., 25 (1977), pp. 220–252.

[17] C. S. Peskin, *The immersed boundary method*, Acta Numer., pp. 1–39, 2002.